Advanced Composite Materials
Publication details, including instructions for authors and subscription information:
http://www.tandfonline.com/loi/tacm20

Evaluating the mechanical properties of a CFRP tube under a lateral impact load using the split Hopkinson bar

Norihiko Taniguchi , Tsuyoshi Nishiwaki & Hiroyuki Kawada

Version of record first published: 02 Apr 2012.

To cite this article: Norihiko Taniguchi , Tsuyoshi Nishiwaki & Hiroyuki Kawada (2005): Evaluating the mechanical properties of a CFRP tube under a lateral impact load using the split Hopkinson bar, Advanced Composite Materials, 14:3, 263-276

To link to this article: http://dx.doi.org/10.1163/1568551054922601

Adv. Composite Mater., Vol. 14, No. 3, pp. 263–276 (2005)

Also available online - www.vsppub.com

Evaluating the mechanical properties of a CFRP tube under a lateral impact load using the split Hopkinson bar

NORIHIKO TANIGUCHI [1,*], TSUYOSHI NISHIWAKI [1] and HIROYUKI KAWADA [2]

[1] *R&D Department, ASCIS Corporation, Kobe, 6-2-1 Takatsukadai, Nishi-ku, Kobe 651-2271, Japan*
[2] *Department of Mechanical Engineering, Waseda University, Tokyo, Japan*

Received 16 April 2004; accepted 30 December 2004

Abstract—The mechanical properties of a CFRP tube, such as strength, stiffness, and energy absorption, are investigated under a lateral impact load using the split Hopkinson pressure bar. In order to obtain the load–displacement curve, a ramped wave was applied to the specimen. It was observed that the ramped incident wave can be used for evaluating the mechanical properties of a CRRP tube under a lateral impact load. The dependence of the displacement rate on the properties mentioned above is also discussed. The result indicates that crack propagation behavior strongly depends on the displacement rate.

Keywords: Split Hopkinson pressure bar; CFRP tube; dynamic behavior; energy absorption; ramped wave.

1. INTRODUCTION

The typical geometry of most general FRP products used in the field of sports is that of a cylindrical tube. In particular, the carbon fiber reinforced plastic (CFRP) tube has been recognized for its high performance and mechanical properties because of which it is utilized in manufacturing baseball bats and golf club shafts [1, 2]. For the practical designing of CFRP tubes for a variety of sporting gear, their mechanical properties under a dynamic load are very important. Nevertheless, an experimental determination of these properties, such as strength, stiffness, and energy absorption, is not an easy task. Several techniques have been developed [3]; for example, the Charpy, Izod, and drop-weight tests, which are typical evaluation methods. However, a few problems have been encountered in these evaluation methods; hence, test results that have been thus obtained can be regarded as semi-empirical, and the generated data may not correlate with each other [4].

*To whom correspondence should be addressed. E-mail: nori@tiger4.sp.asics.co.jp

The split Hopkinson pressure bar (SHPB) method can be used to observe the material's dynamic properties [5–9]. In this technique, the specimen is sandwiched between two long elastic bars, the input and output bars, under dynamic loading conditions. By measuring the axial strain history in both bars, the mechanical properties of the specimen under a dynamic load can be deduced. Although this technique is simple and many researches have been conducted using it [5–15], the technique has not been applied to the study of composite tubes under a lateral impact load to the best of the author's knowledge.

The objective of this study was to apply the SHPB method to the CFRP tube under a lateral impact load. First, the experimental apparatus required for the input and striker bar were constructed, after which the dynamic load–displacement curve was calculated. The fracture behavior of the CFRP tube was also observed using a digital high-speed video system. Next, the dependence of the displacement rate on the CFRP tube mechanical properties, such as strength, stiffness, and energy absorption, is investigated. Finally, the static and dynamic test in terms of crack propagation behavior is discussed based on the fracture surface observation.

2. EXPERIMENTAL

2.1. Specimen

The CFRP tube (volume fraction of fiber, $v_f = 67\%$), which was fabricated by the inner pressure method, was used in this study. Two types of stacking sequence, Type 0: $\theta = 0$ and Type 45: $\theta = \pm 45$, are addressed (Table 1). The geometry and dimensions of the specimen are shown in Fig. 1. The specimens were cut normal to the axial direction, which had a width of 10 ± 0.2 mm.

Table 1.
Stacking sequence of the specimen

Specimen name	Stacking sequence	Thickness (mm)
Type 0	$\theta = 0$ deg	3.0
Type 45	$[+45/-45]_{\text{sym}}$	3.0

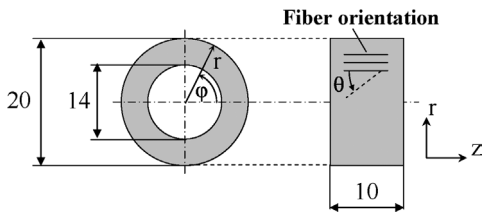

Figure 1. Geometry and dimensions of the CFRP tube fabricated by the inner pressure method.

2.2. Input and striker bar length

In the SHPB system, the load–displacement relationship (*P–u* relationship) can be deduced based on the one-dimensional wave propagation theory [10], such that,

$$u = u_o - u_i = c_0 \int_0^t (-\varepsilon_t + \varepsilon_i - \varepsilon_r)\,\mathrm{d}\tau = -2c_0 \int_0^t \varepsilon_r\,\mathrm{d}\tau, \tag{1}$$

$$P = AE(\varepsilon_i + \varepsilon_r) = AE\varepsilon_t, \tag{2}$$

and

$$\dot{u} = \dot{u}_o - \dot{u}_i = -2c_0\varepsilon_r, \tag{3}$$

where ε_i, ε_r, and ε_t denote the incident, reflected, and transmitted strain waves, respectively; E, A, and c_0 indicate the bar's Young's modulus, cross-sectional area, and elastic wave speed, respectively; u_i and u_o denote the displacement of the specimen interface at the input and output bar sides, respectively. Using equations (1), (2), and (3), the dynamic load–displacement curve can be obtained under a lateral impact load for any given displacement rate $\dot{u}$. A typical example of the strain histories in the input bar is shown in Fig. 2. In this figure, the average strain magnitude $\bar{\varepsilon}_r$ and pulse length Δt correspond to $\dot{u}$ and u, respectively. These parameters can be defined as follows [3]:

$$\bar{\varepsilon}_r = \frac{v_0}{2c_0}, \tag{4}$$

and

$$\Delta t = \frac{2L_0}{c_0}, \tag{5}$$

where v_0 and L_0 denote the striker impact speed and the length of the striker bar, respectively.

The displacement u can be predicted easily from equations (1), (3), (4), and (5), and a simple approximation, such that,

$$u = -\frac{2v_0L_0}{c_0}, \tag{6}$$

and

$$\dot{u} = -v_0. \tag{7}$$

The relationship between L_0 and u is demonstrated in Fig. 3 with several $\dot{u}$. According to the static compression test of the specimen, the maximum displacement $u_{\max}$ is almost 1.0 mm. In this study, in order to obtain an identical displacement, L_0 is required to be 1500 mm or more.

There is another important issue that needs to be addressed. The input bar length L_1 must be designed sufficiently long so as to avoid the overlap between the incident

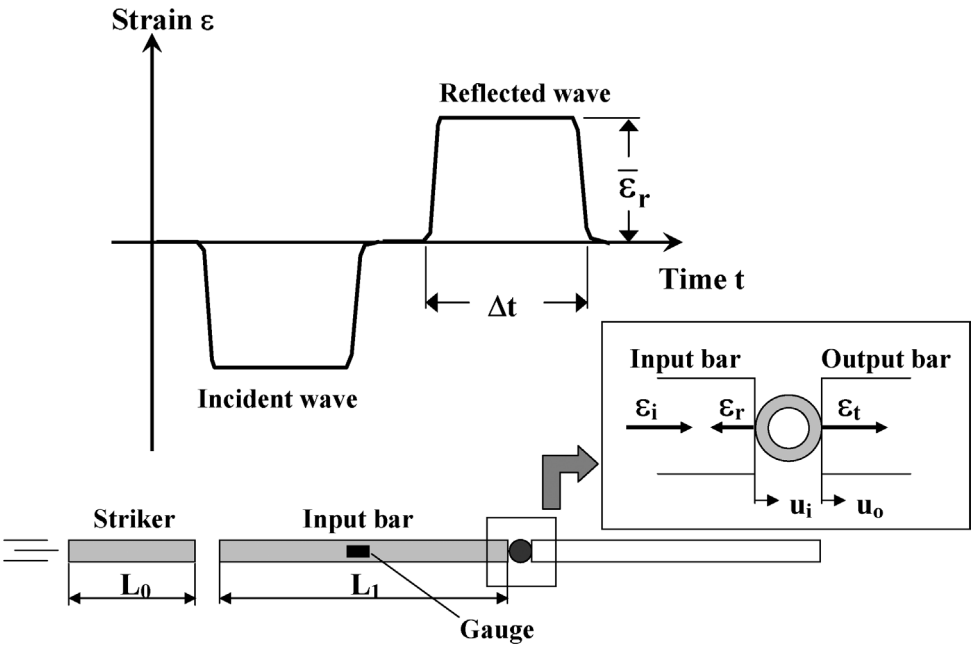

Figure 2. Typical example of the strain histories in the input bar.

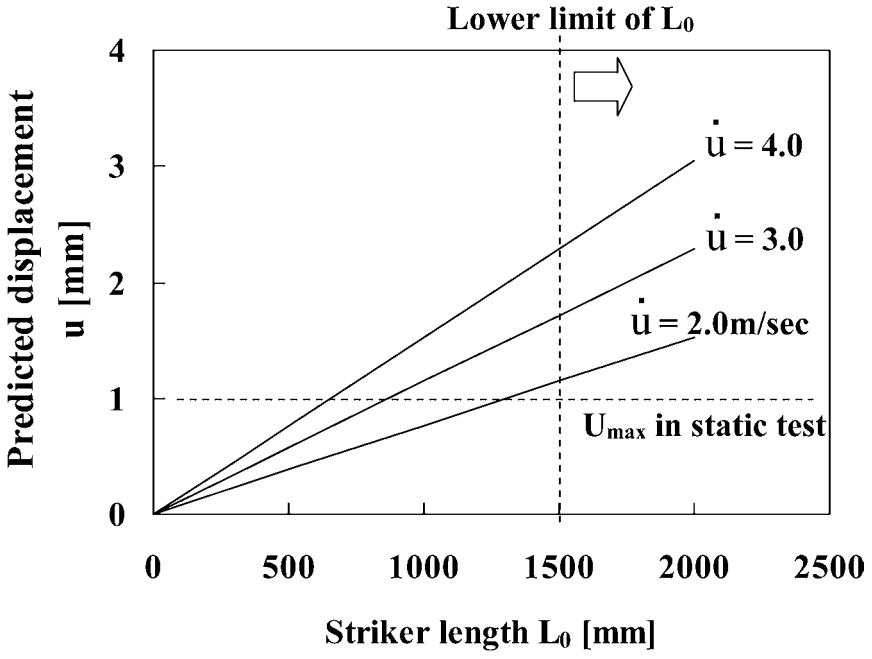

Figure 3. The relationship between L_0 and u with several $\dot{u}$.

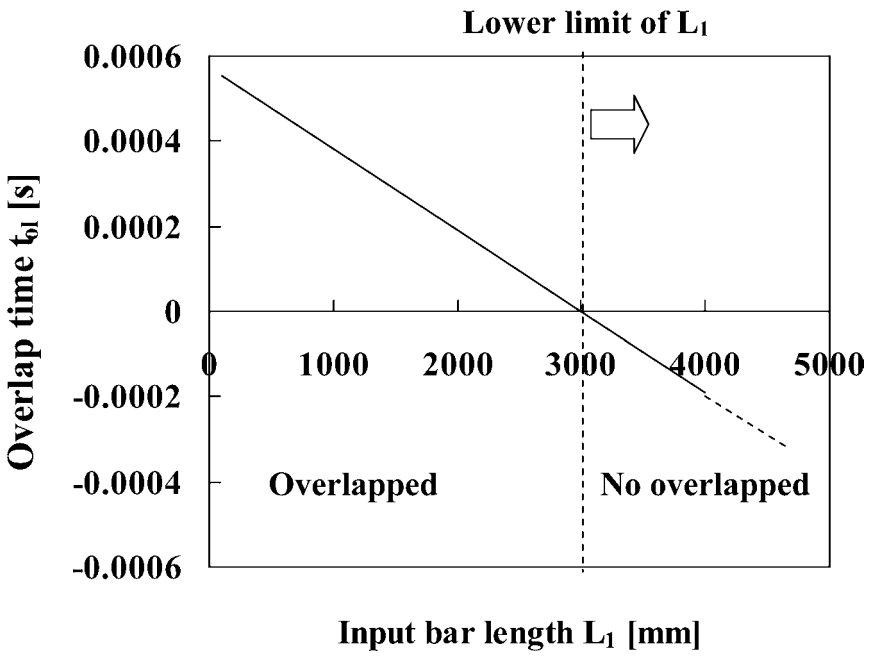

Figure 4. Relationship between L_1 and t_{ol}. The lower-limit length of the input bar, L_1, is 3000 mm.

wave and the reflected wave. The overlapped time length t_{ol} is given by,

$$t_{ol} = \Delta t - c_0 L_1 = \frac{2L_0}{c_0} - \frac{L_1}{c_0}. \tag{8}$$

The result, which is obtained for $L_0 = 1500$ mm, shows that the lower-limit length of the input bar, L_1, is 3000 mm (Fig. 4).

2.3. Experimental system

The SHPB system, which was assembled in our laboratory, is shown in Fig. 5. It consists of the striker bar ($L_0 = 1500$ mm, $d_0 = 16$ mm, steel); the input bar ($L_1 = 4000$ mm, $d_1 = 16$ mm, steel); and the output bar ($L_2 = 1500$ mm, $d_2 = 16$ mm, steel). In order to observe the fracture behavior of the tubular CFRP specimen, a digital high-speed video camera (NAC fx-6000, sampling at the rate of 10 kHz) was also provided in front of the specimen. The specimen was located lateral to the loading direction and was sandwiched between the input and output bars. Once the striker bar hits the input bar, a compression wave is generated. At the point of contact of the specimen and the input bar, a part of this wave is transmitted into the specimen and the output bar, while the remainder is reflected back to the input bar. The data obtained from the SHPB method comprise the strain histories of the input and output bars. In the present study, the strain histories are recorded from the strain gauges (input bar: KFG-1-350-C1-11, output bar: KSP-1-350-E4, upper frequency limit: 500 kHz) at a sampling rate of 1.0 MHz via a DC

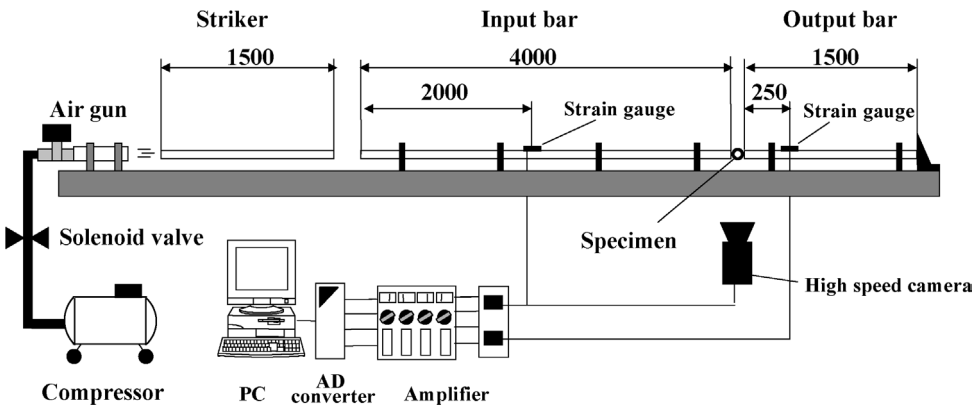

Figure 5. The SHPB system.

amplifier (upper frequency limit: 100 kHz). Also, previous studies conducted using the PMMA tube, which has lower stiffness and density than those of Type 0 and Type 45, have confirmed that the effect of impedance matching on measurement accuracy is negligible.

3. EXPERIMENTAL RESULTS

3.1. Load–displacement curve

The dynamic load–displacement curve (*P–u* curve) can be obtained from strain-gauge outputs and equations (1)–(3). A typical example of a *P–u* curve for Type 0 is shown in Fig. 6 with the displacement rate history. As is clearly shown in this figure, the resulting curve shows large fluctuations, even at the initial stage. This behavior is caused by the inertial force, which is due to a steep increase in the displacement rate at the initial stage. In order to discuss the mechanical properties under a lateral impact load in detail as a function of time, this fluctuating behavior must be controlled.

3.2. Application of a ramped incident wave

Several techniques have been proposed to control the fluctuating behavior of the response [11–15]. In this study, a piece of zinc (diameter $\varnothing = 13$ mm, thickness $h = 3.0$ mm) is sandwiched between the striker and input bars, from the work of Ogawa *et al.* [14, 15]. Hence, the ramped incident wave is produced by the plastic deformation of zinc. Typical examples of strain-gauge outputs that are produced using zinc are shown in Fig. 7a and b. In these figures, the strain-gauge outputs obtained from the general SHPB method are also demonstrated (dashed line). Further, the time-frequency analysis of the incident wave is carried out using the wavelet transformation (Fig. 8). A comparison of the two results reveals that the higher-frequency wave at the initial rising stage is eliminated by the zinc insertion.

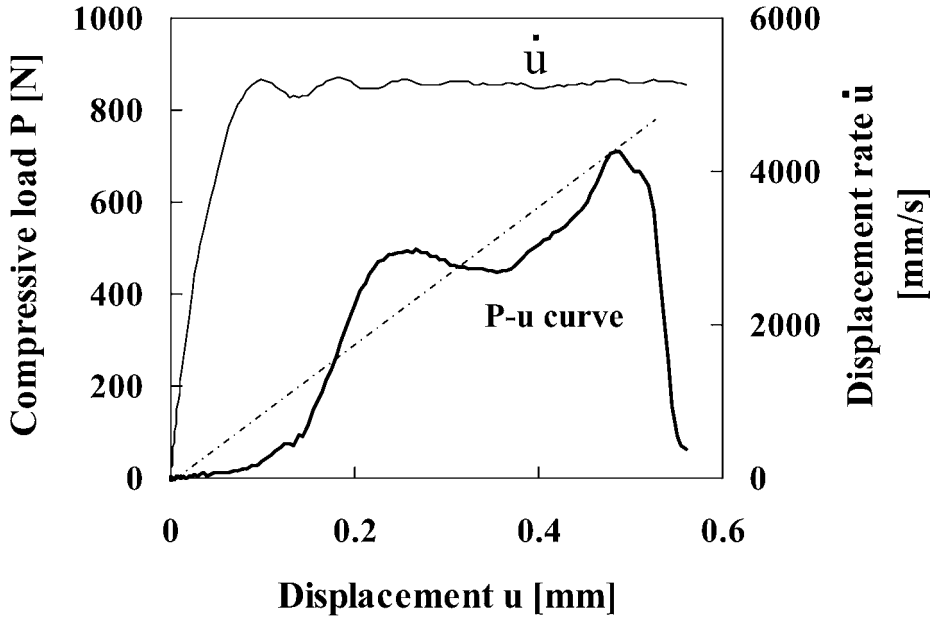

Figure 6. A typical example of a *P–u* curve for Type 0.

The dynamic *P–u* curve was re-calculated using the strain-gauge outputs shown in Fig. 7. The resulting curve and the displacement rate history are shown in Fig. 9a. It is obvious that the fluctuating behavior is almost controlled. This result suggests that the ramped incident wave is applicable for evaluating the mechanical properties of a CFRP tube under a lateral impact load. A series of fracture progressive photographs are also shown in Fig. 9b. The letters in the *P–u* curve correspond to each photograph. In the case of Type 0, the transverse crack is initiated in the boxed area (C1). Subsequently, this crack propagates in thickness direction. Finally, the specimen is split into four pieces (D1 and E1). A comparison of these photographs with the *P–u* curve makes it clear that when the load reached the maximum point, the crack was initiated. The dominant failure mode that affects the $P_{\max}$ is the matrix fracture.

Both the dynamic *P–u* curve and the fracture process for Type 45 obtained from the application of the ramped incident wave are shown in Fig. 10. The important point to be noted in this figure is that the reduction in the lateral compressive stiffness, P/u, can be observed for a particular load; namely, the *P–u* curve of Type 45 can be divided into two stages — linear and non-linear. This reduction is caused by increase in damage due to the matrix crack. It was impossible to observe this from the photograph (B2). However, just before $P_{\max}$, delamination can be confirmed (C2). This result implies that the dominant failure mode, which affects the $P_{\max}$ of Type 45, is an inter-laminar delamination. Moreover, this delamination position is far from the contact area in the hoop direction. This phenomenon is caused by the coupling effect.

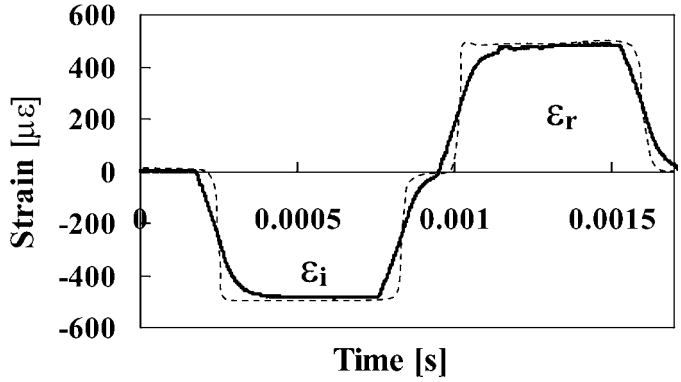

(a)

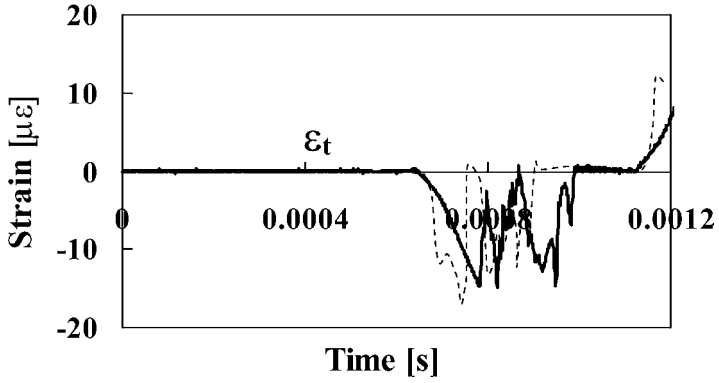

(b)

Figure 7. Typical examples of strain-gauge outputs; solid line: using zinc; dashed line: without zinc. (a) Input and reflected wave, (b) output wave.

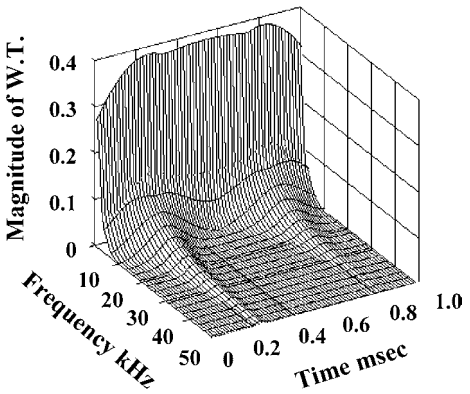

(a) Rectangular incident wave (without Zn)

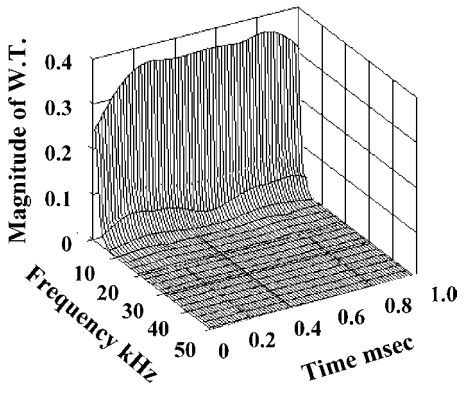

(b) Ramped incident wave (with Zn)

Figure 8. Time-frequency analysis of the incident wave carried out using the wavelet transformation.

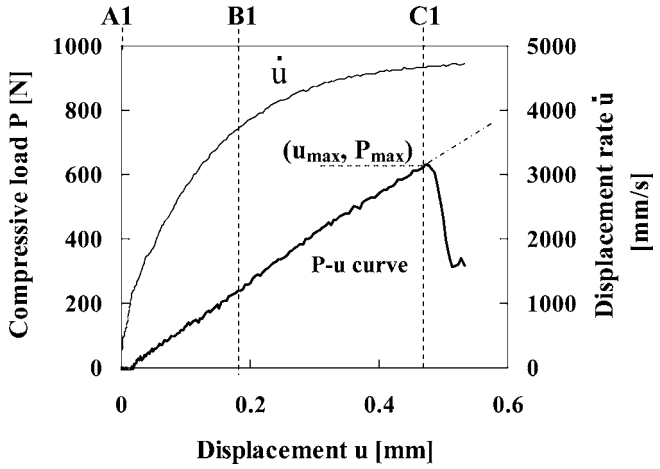

(a)

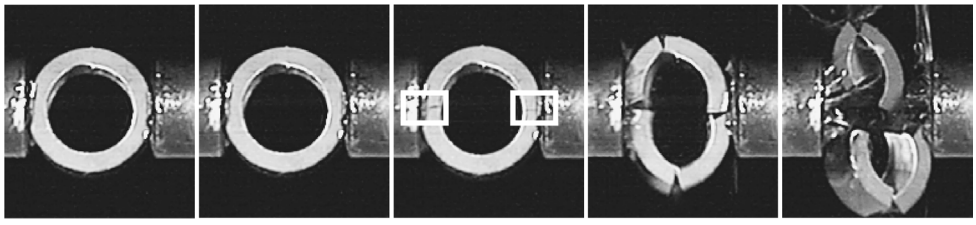

(b)

Figure 9. (a) The resulting curve and the displacement rate history when the dynamic P–u curve was re-calculated using the strain-gauge outputs. (b) Succesive photographs of fracture in CFRP tube (Type 0). A1, B1 and C1 correspond to the displacements in (a).

4. DISCUSSION

4.1. Dependence of displacement rate on the lateral compressive stiffness, load, and displacement

In order to investigate the dependence of displacement rate on the mechanical properties of the specimen, the lateral compressive stiffness (P/u), load ($P_{\max}$, P_1, and P_2), and displacement ($u_{\max}$, u_1, and u_2) under various displacement rates are measured. The relationships between $\dot{u}$ and the above parameters are shown in Fig. 11a–c. In Type 0 and the linear stage of Type 45 (Fig. 11a and b), all these parameters increase with $\dot{u}$. It can be said without difficulty that the increase in these tendencies is primarily due to the viscoelasticity of the matrix [3, 7]. On the other hand, in the non-linear stage of Type 45, it is clear that displacement u_2 decreases with $\dot{u}$ despite the fact that P_2 is almost identical. This implies that the fracture behaviors under a dynamic load become more brittle rather than those under static loads.

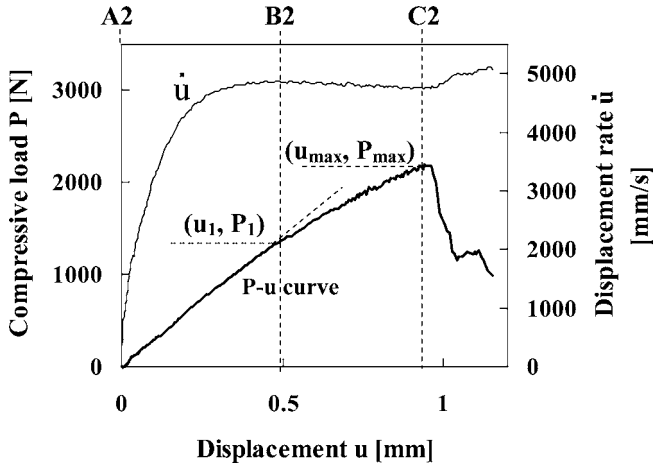

(a)

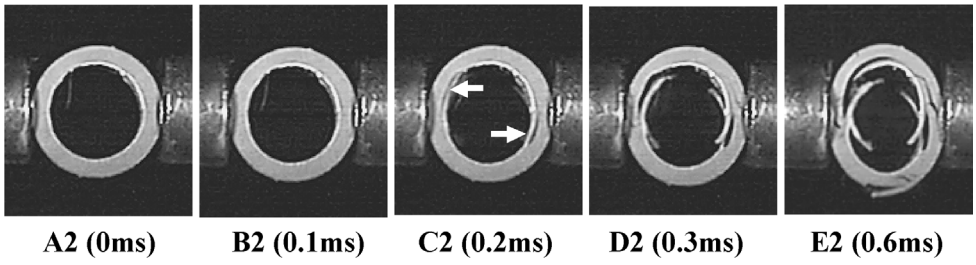

(b)

Figure 10. The dynamic P–u curve and the fracture process for Type 45 obtained from the application of the ramped incident wave. (a) Load–displacement curve, (b) successive photographs of fracture in CFRP tube; A2, B2 and C2 correspond to the displacements in (a).

4.2. Dependence of displacement rate on energy absorption mechanism

The absorbed energy U_0 is calculated for various displacement rates $\dot{u}$. In this study, the U_0 is defined as the energy that is absorbed up to the maximum load point.

The U_0 is given by,

$$U_0 = \int_0^{u_{\max}} P \, \mathrm{d}u. \tag{9}$$

The U_0 for Type 0 and Type 45 are plotted as a function of $\dot{u}$ in Fig. 12a and b, respectively. In Type 0, the U_0 increases with $\dot{u}$. This tendency is caused by the increase in the values of $P_{\max}$, $u_{\max}$, and *(P/u)*, which are described in Section 4.1. Specifically, the viscoelasticity of the matrix has a major influence on the U_0 of Type 0. On the other hand, in Type 45, the U_0 has an almost constant value in the range of 0–5000 mm/s. As already demonstrated, the P–u curve of Type 45 comprises the linear and non-linear stages. Therefore, it is possible to calculate the

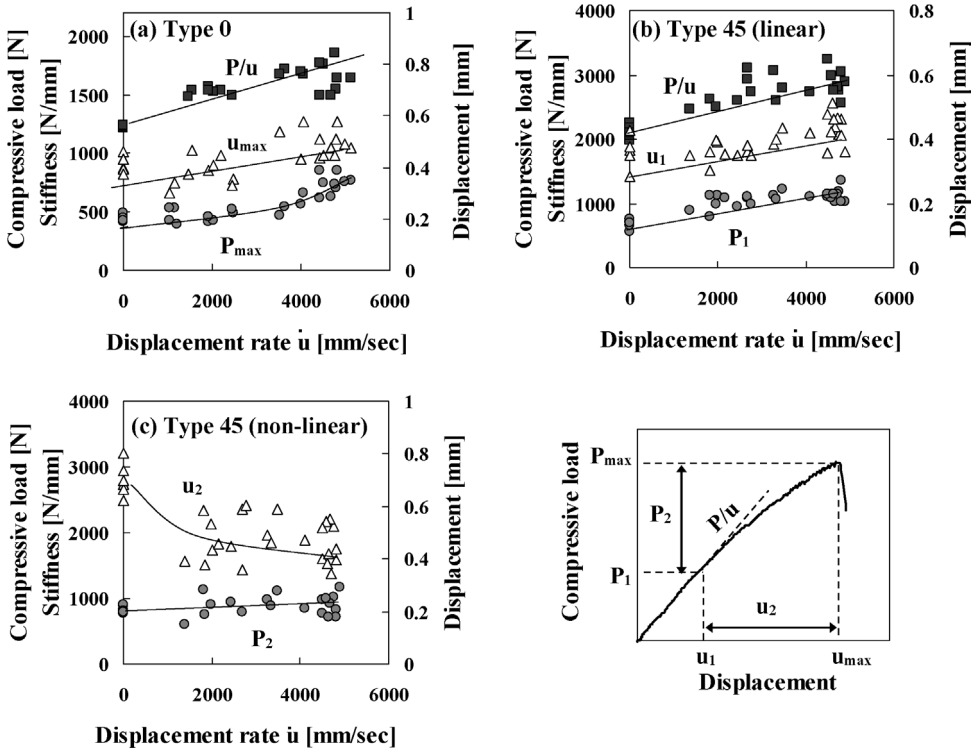

Figure 11. The relationships between the displacement rate $\dot{u}$ and the lateral compressive stiffness (P/u), load ($P_{\max}$, P_1, and P_2), and displacement ($u_{\max}$, u_1, and u_2) for Type 0 and Type 45 (linear and non-linear).

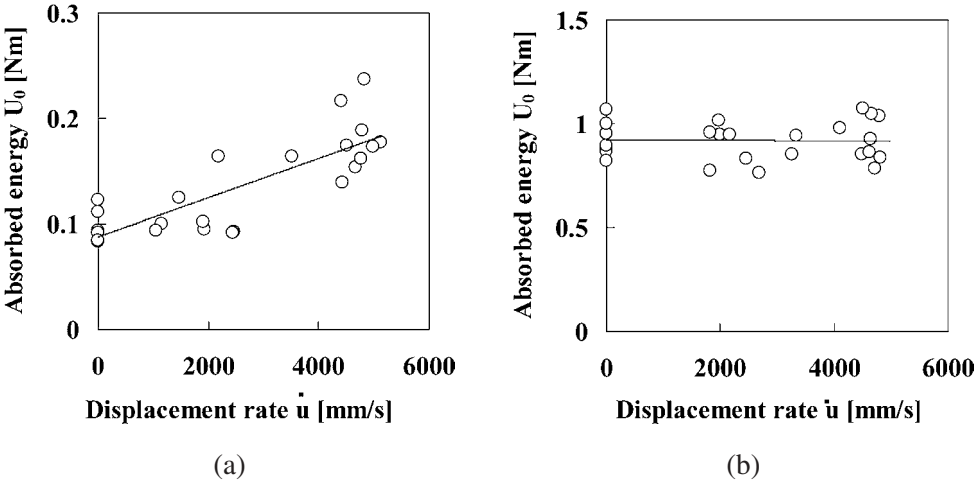

Figure 12. The relationship between the absorbed energy U_0 and the displacement rate $\dot{u}$ for Type 0 (a) and Type 45 (b).

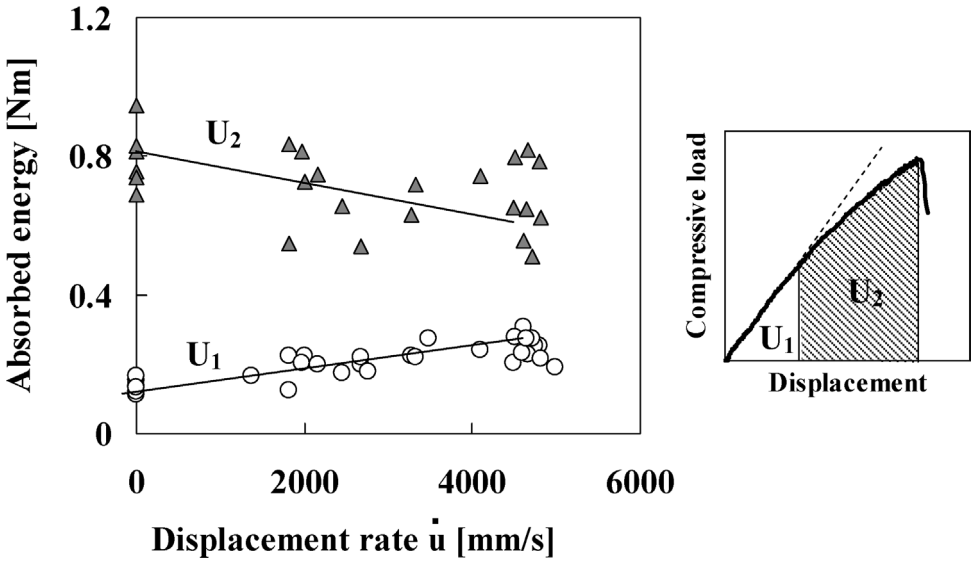

Figure 13. The calculated absorbed energies for the linear and non-linear stages (U_1 and U_2).

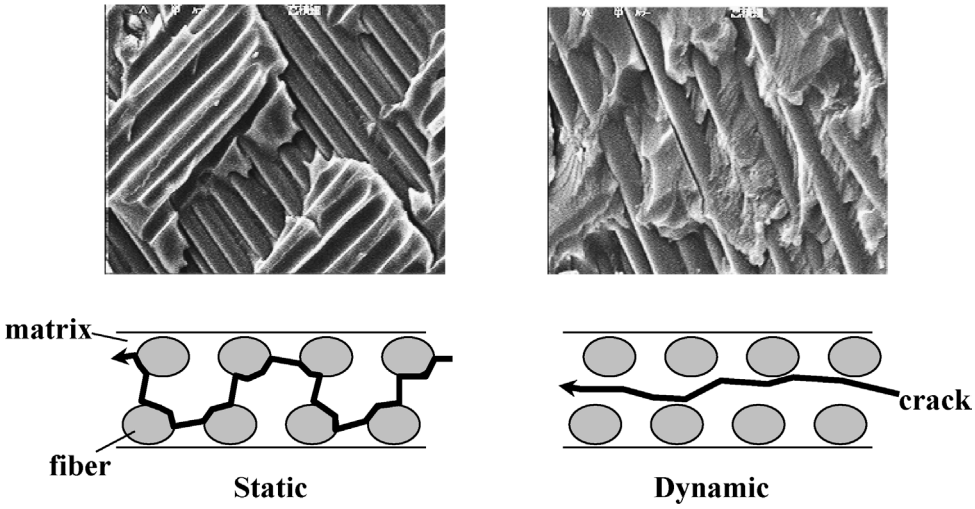

Figure 14. Comparison of the fracture surface behavior between the static and the dynamic test.

absorbed energy in each stage. The calculated absorbed energies for the linear and non-linear stages (U_1 and U_2) are shown in Fig. 13 as a function of $\dot{u}$. The U_1 and U_2 correspond to the absorbed energy before and after the onset of the matrix crack, respectively. They are given by,

$$U_1 = \int_0^{u_1} P \, \mathrm{d}u, \tag{10}$$

and

$$U_2 = \int_{u_1}^{u_{\max}} P \, \mathrm{d}u. \tag{11}$$

As is clearly shown in Fig. 13, the U_1 increases with $\dot{u}$. This phenomenon is due mainly to the viscoelasticity of the matrix as well as that of Type 0. However, it is shown that the U_2 decreases with an increasing $\dot{u}$. In order to clarify the damage propagation mechanism of Type 45 more precisely, the fracture surface observation is performed by using a scanning electron microscope (SEM). Typical examples of a fracture surface under static and dynamic loads, whose displacement rates are 1.67×10^{-5} mm/s and 5.0×10^{3} mm/s, respectively, are shown in Fig. 14. In the case of the static test, it is clear that the crack propagates along the interface between the fiber and the matrix. On the other hand, in the fracture surface of the dynamic test, a number of hackles exist in the matrix area, i.e. the crack propagation area consists of not only the interface between the fiber and the matrix but also the matrix itself. This result is associated with the strain rate dependency of the fracture toughness of Epoxy resin [16].

5. CONCLUSIONS

The following conclusions can be drawn from this work.

(1) By using the ramped wave, it was confirmed that the SHPB method is applicable for evaluating the mechanical properties of a CFRP tube under lateral impact load.

(2) In Type 0 and the linear stage of Type 45, the lateral compressive stiffness (P/u), load ($P_{\max}$ and P_1), and displacement ($u_{\max}$ and u_1) increase with $\dot{u}$. This is due mainly to the viscoelasticity of the matrix.

(3) In the non-linear stage of Type 45, displacement (u_2) decreases with increasing $\dot{u}$ even though the load (P_2) is almost identical. This result implies that the fracture behaviors become more brittle under a dynamic load than under a static load.

(4) The total absorbed energy U_0 of Type 0 increases with $\dot{u}$ due to the viscoelasticity of the matrix. However, the U_0 of Type 45 has an almost constant value.

(5) The U_0 of Type 45 is divided into two stages, U_1 and U_2. Due to the viscoelasticity of the matrix, the U_1 increases with $\dot{u}$. On the other hand, the U_2 decreases with increasing $\dot{u}$. This is caused by the dependence of the strain rate on the fracture toughness of epoxy resin.

Acknowledgements

It is our pleasure to acknowledge our beneficial discussions with Dr. K. Ogawa, Kyoto University.

REFERENCES

1. T. Nishiwaki, A. Yokoyama, Z. Maekawa, H. Hamada and S. Mori, A quasi-three-dimensional lateral compressive analysis method for a composite cylinder, *Compos. Struct.* **32**, 293–298 (1995).
2. T. Nishiwaki, Designing of CFRP baseball bats, *SAMPE Journal* **38**, 80–82 (2002).
3. R. L. Sierakowski and S. K. Chaturvedi, in: *Dynamic Loading and Characterization of Fiber-reinforced Composites*, Chapter 2, John Wiley (1997).
4. S. N. Kakarala and J. L. Roche, Experimental comparisons of several impact test methods, *ASTM STP* **936** (1986).
5. E. D. H. Davies and S. C. Hunter, The dynamic compression testing of solids by the method of the split Hopkinson pressure bar, *J. Mech. Phys. Solids* **11**, 155–179 (1963).
6. K. Kobayashi, Y. Tanabe and T. Hara, Mechanical behavior of bovine trabecular bone subjected to impact compressive load, *Trans. Jpn. Soc. Mech. Eng. A* **63**, 160–166 (1997).
7. N. Takeda, L. Wan, M. Hiramatsu and J. Yuan, Characterization of effects of strain rate and temperature on impact compressive damage progress of glass fiber reinforced composites, *Trans. Jpn. Soc. Mech. Eng. A* **63**, 134–139 (1997).
8. C. K. H. Dharan and F. E. Hauser, Determination of stress-strain characteristics at very high strain rates, *Exp. Mech*. **10**, 370 (1970).
9. Y. Yokoyama, Impact tension and compression testing of ductile cast iron with split Hopkinson bar, *J. Soc. Mater. Sci. Japan* **45**, 785–791 (1996).
10. K. F. Graff, *Wave Motion in Elastic Solids*, Dover Publications (1991).
11. T. Fukuda, T. Fujii, M. Miki and H. Yoshida, *J. Soc. Mater. Japan* **28**, 1193 (1979).
12. Y. Yamauchi, T. Kurokawa and T. Kusaka, Estimation of dynamic interlaminar fracture toughness of CFRP by ENF test using SHPB method, *J. Soc. Mater. Sci. Japan* **42**, 1445–1451 (1993).
13. T. Kusaka, T. Kurokawa and Y. Yamauchi, Strain rate dependence of mode II interlaminar fracture toughness of unidirectional CF/Epoxy composite laminates, *J. Soc. Mater. Sci. Japan* **43**, 445–450 (1994).
14. K. Ogawa, A. Kuraishi, T. Nishida and F. Sugiyama, Impact three-point bending test of a continuous carbon fiber-reinforced silicon nitride, *J. Soc. Mater. Sci. Japan* **45**, 799–804 (1996).
15. F. Higashida, and K. Ogawa, Impact three-point bending tests on FRP by split-Hopkinson Bar technique, *J. Soc. Mater. Sci. Japan* **39**, 1462–1468 (1990).
16. A. J. Kinloch and R. J. Young, *Fracture Behavior of Polymers*. Elsevier (1983).